Available online at www.sciencedirect.com
ScienceDirect
Journal of Sound and Vibration 309 (2008) 794–804
JOURNAL OF SOUND AND VIBRATION
www.elsevier.com/locate/jsvi

A modified axisymmetric finite element for the 3-D vibration analysis of piezoelectric laminated circular and annular plates

Chorng-Fuh Liu*, Ting-Jung Chen, Ying-Jie Chen

Department of Mechanical and Electro-Mechanical Engineering, National Sun Yat-Sen University, Kaohsiung, Taiwan, ROC

Received 29 June 2006; received in revised form 4 May 2007; accepted 28 July 2007
Available online 29 September 2007

Abstract

A finite element is presented to analyze the three-dimensional (3-D) vibration of piezoelectric coupled circular and annular plates. The proposed finite element is a modification of a conventional axisymmetric finite element and is capable of conducting both axisymmetric and nonaxisymmetric vibration analysis of circular and annular laminated plates, with piezoelectric layers therein. The present formulation, a two-dimensional model itself, can investigate 3-D vibration of those plates for a preselected number of nodal diameters, and is therefore more economical than the conventional 3-D finite element analysis, yet still has almost the same accuracy and versatility as the 3-D analysis. In cases such as analysis of stators of traveling wave ultrasonic motors where only vibration modes with particular numbers of nodal diameters are of interest, the proposed approach is very convenient and useful.

1. Introduction

Circular and annular plates of piezoelectric materials or their laminations with other materials are becoming more and more important machine or electric elements, especially in sensors and actuators. To take good advantage of these materials, a thorough understanding of the behaviors of those plates is a necessity. Among them, the vibration characteristics are probably most important and are studied most often due to the fact that many applications use the resonant characteristics of piezoelectric circular and annular plates.

Most of the techniques used to analyze the vibration of piezoelectric circular and annular plates can be classified into two categories: one is based on plate theories, such as Wang et al. [1], Huang [2], Hadegorn and Wallaschek [3], Hagood and McFarland [4], Hagedorn et al. [5], Friend and Stutts [6], and Ming and Peiwen [7]. In these researches, vibrations of piezoelectric circular plate or its lamination with elastic plate have been analyzed by classical plate theories, which neglect transverse shear deformation and, in most of the cases, rotary inertia except [3]. Liu et al. [8] then applied a first-order shear deformation plate theory, which considered transverse shear deformation and rotary inertia in some way, to investigate vibration of piezoelectric coupled moderately thick circular plates. Duan et al. [9] have studied vibration of piezoelectric coupled thin and thick annular plates based on both classical and Mindlin plate theories and derived analytic

*Corresponding author. Fax: +886 7 5254299.
E-mail address: liucf@mail.nsysu.edu.tw (C.-F. Liu).

0022-460X/$ - see front matter © 2007 Elsevier Ltd. All rights reserved.
doi:10.1016/j.jsv.2007.07.048

solutions. The other category are of three-dimension-elasticity-based analyses, including the two-dimensional (2-D) axisymmetric analyses such as Kagawa and Yamabuchi [10], Adelman et al. [11], Guo et al. [12], and Kunkel et al. [13], which are all axisymmetric finite element analyses. Heyliger and Ramirez [14] have combined finite element method (thickness direction) and Ritz method (radial direction) to model the vibration of laminated circular piezoelectric plates. Exact three-dimensional (3-D) axisymmetric vibration analyses for transversely isotropic piezoelectric circular plates under particular types of boundary conditions have been conducted by Ding et al. [15]. Results of vibration frequencies obtained from 3-D finite element analyses, which can study axisymmetric and nonaxisymmetric vibrations, are presented in Ref. [16] by Lin and Ma and also in Ref. [9], and are compared with those of experiments [16] and different plate theories [9], respectively.

Plate-theory-based approaches are simple from view point of analysis and is economical in computation because of its 2-D nature. However, accuracy of classical-plate-theory results degrades when plate thickness becomes larger due to their assumptions and approximations. Shear deformation theories have been evolved to overcome the shortcomings of the classical ones and is usually proved to be superior. Nevertheless, they overestimate in some cases and underestimate in other cases. On the contrary, analyses based on the 3-D theory are most general and can reveal every aspects of vibration behaviors. However, they are also hard to solve analytically for most of the cases and are very time-consuming to solve the problems numerically, not mentioning the enormous output from which meaningful results can be extracted and interpreted only with greater effort.

In the present study, a finite element is developed, which is a modification of a previous one [17] by including the piezoelectric effect. The present element has the capability to conduct 3-D axisymmetric and nonaxisymmetric vibration analysis of piezoelectric coupled circular and annular plates, yet still remains itself a 2-D approach. Since it analyzes directly the vibration frequencies and modes with a specific number of nodal diameters, the proposed approach could be especially useful for the design of traveling wave ultrasonic motors and the likes where the actuated traveling wave is formed by simultaneously exciting two standing waves which have the same, selected number of nodal diameters and are out of phase temporally and spatially [18].

2. Formulation

The field variables are assumed as follows:

$$\begin{aligned} u_r(r,\theta,z,t) &= u(r,z)\cos n\theta \sin \omega t,\\ u_\theta(r,\theta,z,t) &= v(r,z)\sin n\theta \sin \omega t,\\ u_z(r,\theta,z,t) &= w(r,z)\cos n\theta \sin \omega t,\\ \phi(r,\theta,z,t) &= \Phi(r,z)\cos n\theta \sin \omega t. \end{aligned} \tag{1}$$

u_r, u_θ, u_z are displacements in the radial, tangential, and thickness directions of circular plates, and r, θ, z are the corresponding coordinates when a cylindrical coordinate system is used. t is time. n is number of nodal diameters. ω is vibration frequency in radians/s. Electric potential ϕ also appears as dependent variable because of the inclusion of piezoelectric effect. Synchronous motion is assumed as always.

The above formulae are a modification of a previous research on vibration of circular and annular plates [17] by taking the electromechanical effect into consideration. They are also the same as those shown in Ref. [14].

For a piezoelectric material, the electromechanical constitutive equations are:

$$\begin{aligned} \{T\} &= [C]\{S\} - [e]^{\mathrm{T}}\{E\},\\ \{D\} &= [e]\{S\} + [\varepsilon]\{E\}, \end{aligned} \tag{2}$$

where $\{T\}$, $\{S\}$, and $\{E\}$ are 6×1 vectors of stresses, strains and a 3×1 vector of electric fields, respectively. $\{D\}$ is vector of electric displacements. $[C]$ is elastic stiffness matrix at constant electric fields and $[\varepsilon]$ is dielectric matrix at constant strain. $[e]$ is piezoelectric matrix. Superscript T represents transpose.

For a hexagonal crystal (6 mm) piezoelectric ceramics poling in the z-direction, the elastic stiffness matrix, the piezoelectric matrix and the dielectric matrix have the following forms:

$$[C]=\begin{bmatrix} c_{11} & c_{12} & c_{13} & 0 & 0 & 0 \\ c_{12} & c_{22} & c_{23} & 0 & 0 & 0 \\ c_{13} & c_{23} & c_{33} & 0 & 0 & 0 \\ 0 & 0 & 0 & c_{44} & 0 & 0 \\ 0 & 0 & 0 & 0 & c_{55} & 0 \\ 0 & 0 & 0 & 0 & 0 & c_{66} \end{bmatrix},$$

$$[e]=\begin{bmatrix} 0 & 0 & 0 & 0 & e_{15} & 0 \\ 0 & 0 & 0 & e_{24} & 0 & 0 \\ e_{31} & e_{32} & e_{33} & 0 & 0 & 0 \end{bmatrix},$$

$$[\varepsilon]=\begin{bmatrix} \varepsilon_{11} & 0 & 0 \\ 0 & \varepsilon_{22} & 0 \\ 0 & 0 & \varepsilon_{33} \end{bmatrix} \tag{3}$$

with $c_{11}=c_{22}$, $c_{13}=c_{23}$, $c_{44}=c_{55}$, $c_{66}=(c_{11}-c_{12})/2$, $e_{24}=e_{15}$, $e_{31}=e_{32}$, and $\varepsilon_{11}=\varepsilon_{22}$.

The above constitutive equations apply to layers of piezoelectric material. For the elastic layer to which the piezoelectric layers stick, the proper constitutive equation should be used and only the stiffness matrix appears without the piezoelectric and the dielectric ones

The strain–displacement relations are defined as

$$\{S\}=\begin{Bmatrix} s_1 \\ s_2 \\ s_3 \\ s_4 \\ s_5 \\ s_6 \end{Bmatrix}=\begin{Bmatrix} \varepsilon_r \\ \varepsilon_\theta \\ \varepsilon_z \\ \gamma_{z\theta} \\ \gamma_{rz} \\ \gamma_{r\theta} \end{Bmatrix}=\begin{Bmatrix} \dfrac{\partial u_r}{\partial r} \\ \dfrac{u_r}{r}+\dfrac{1\partial u_\theta}{r\,\partial\theta} \\ \dfrac{\partial u_z}{\partial z} \\ \dfrac{\partial u_\theta}{\partial z}+\dfrac{1\partial u_z}{r\,\partial\theta} \\ \dfrac{\partial u_r}{\partial z}+\dfrac{\partial u_z}{\partial r} \\ \dfrac{\partial u_\theta}{\partial r}-\dfrac{u_\theta}{r}+\dfrac{1\partial u_r}{r\,\partial\theta} \end{Bmatrix} \tag{4}$$

and the six stress components in the stress vector are $T_1=\sigma_r$, $T_2=\sigma_\theta$, $T_3=\sigma_z$, $T_4=\tau_{z\theta}$, $T_5=\tau_{rz}$, and $T_6=\tau_{r\theta}$.

The electric field-potential relation is also needed

$$\{E\}=\begin{Bmatrix} E_1 \\ E_2 \\ E_3 \end{Bmatrix}=\begin{Bmatrix} E_r \\ E_\theta \\ E_z \end{Bmatrix}=\begin{Bmatrix} -\dfrac{\partial\phi}{\partial r} \\ -\dfrac{1\partial\phi}{r\,\partial\theta} \\ -\dfrac{\partial\phi}{\partial z} \end{Bmatrix}. \tag{5}$$

The variational form for a piezoelectric material is

$$0 = \int_{t_0}^{t} \mathrm{d}t \int_{v} [T_i\,\delta s_i + D_j\,\delta E_j + \rho \ddot{u}_k\,\delta u_k]\,\mathrm{d}v,$$
$$i = 1{-}6, \quad j = 1{-}3, \quad k = r, \theta, z, \tag{6}$$

where the double dot denotes acceleration.

After substituting Eqs. (1)–(5) into Eq. (6), all the terms in the variational form are expressed in the three displacements and the electric potential which, as in the conventional finite element procedure, are substituted further with

$$u(r,z) = \sum_{1}^{nd} N_i u_i,$$
$$v(r,z) = \sum_{1}^{nd} N_i v_i,$$
$$w(r,z) = \sum_{1}^{nd} N_i w_i,$$
$$\Phi(r,z) = \sum_{1}^{nd} N_i \phi_i,$$

where N_i is shape function and u_i, v_i, w_i, ϕ_i are nodal values of the dependent variables. nd is the number of nodes in an element.

The following elemental equation is thus obtained:

$$\begin{bmatrix} [k_{uu}] & [k_{u\phi}] \\ [k_{\phi u}] & [k_{\phi\phi}] \end{bmatrix} \begin{bmatrix} \{U_e\} \\ \{\Phi_e\} \end{bmatrix} = \omega^2 \begin{bmatrix} [m_{uu}] & [0] \\ [0] & [0] \end{bmatrix} \begin{bmatrix} \{U_e\} \\ \{\Phi_e\} \end{bmatrix}$$

where $\{U_e\} = [u_1 u_2 \ldots u_{nd} \quad v_1 v_2 \ldots v_{nd} \quad w_1 w_2 \ldots w_{nd}]^{\mathrm{T}}$ and $\{\Phi_e\} = [\phi_1 \phi_2 \cdots \phi_{nd}]^{\mathrm{T}}$. Expressions for the stiffness matrix $[k_{uu}]$, the piezoelectric matrix $[k_{u\phi}] = [k_{\phi u}]^{\mathrm{T}}$, the dielectric matrix $[k_{\phi\phi}]$, and the mass matrix $[m_{uu}]$ are shown in the appendix.

After assembling the above equations for all the elements in the mesh, system equation is derived as follows:

$$\begin{bmatrix} [K_{uu}] & [K_{u\phi}] \\ [K_{u\phi}]^{\mathrm{T}} & [K_{\phi\phi}] \end{bmatrix} \begin{bmatrix} \{U\} \\ \{\Phi\} \end{bmatrix} = \omega^2 \begin{bmatrix} [M_{uu}] & [0] \\ [0] & [0] \end{bmatrix} \begin{bmatrix} \{U\} \\ \{\Phi\} \end{bmatrix}.$$

For free vibration analysis, the electric potential on the electroded surfaces of the piezoelectric layers are set to zero, and these boundary conditions on ϕ can be imposed on the top and bottom surfaces of the piezoelectric circular layers in the following way: the rows of $[K_{u\varphi}]^{\mathrm{T}}$ and $[K_{\varphi\varphi}]$, and the columns of $[K_{u\varphi}]$ and $[K_{\varphi\varphi}]$ corresponding to the specified zero nodal potential degrees of freedom are set to zero first, then the corresponding diagonal entries in $[K_{\varphi\varphi}]$ are set to 1. We end up with the following equation with all the zero potential boundary conditions satisfied:

$$\begin{bmatrix} [K_{uu}] & [K^*_{u\phi}] \\ [K^*_{u\phi}]^{\mathrm{T}} & [K^*_{\phi}] \end{bmatrix} \begin{bmatrix} \{U\} \\ \{\Phi\} \end{bmatrix} = \omega^2 \begin{bmatrix} [M_{uu}] & [0] \\ [0] & [0] \end{bmatrix} \begin{bmatrix} \{U\} \\ \{\Phi\} \end{bmatrix}. \tag{7}$$

For the elastic layers, the electromechanical effects are not considered at all. The present formulation becomes the one shown in Ref. [17] where only $[K_{uu}]$, $[M_{uu}]$, and $[U]$ are nonzero, and the validity and accuracy of the present approach for pure elastic material has also been demonstrated in Ref. [17].

Eq. (7) cannot be solved directly to get the vibration frequencies due to the appearance of the zero matrices. A static condensation of the electric potential degrees of freedom is conducted as in Ref. [19] and the following

equation is obtained:

$$\left([K_{uu}] - [K^*_{u\phi}][K^*_{\phi\phi}]^{-1}[K^*_{u\phi}]^{\mathrm{T}}\right)[U] = \omega^2[M_{uu}][U].$$

This is the equation that we use to solve the natural frequency ω. The mechanical boundary conditions are imposed in the usual way of the finite element method.

3. Results and discussions

To test the validation and accuracy of the present element, three cases are analyzed and compared with the literature. The first one is a wholly piezoelectric circular plate of PIC-151 with diameter 30 mm, thickness 1 mm, completely coated with electrodes on both surfaces and of free boundary condition. Table 1 lists the material properties. Results of the present method are compared with those of a 3-D finite element solution by ABAQUS and experiments [16]. High accuracy of the present method is demonstrated by the excellent agreement between ABAQUS 3-D solutions and the present ones, as shown in Table 2. In the table, mode nos. 3–6 with $n = 0$ are of in-plane modes while the others are all out-of-plane modes. Some other modes lying in between those shown in Table 2 are also derived in the present study. They are not presented here because there are no counterparts in Ref. [16] to compare with.

The second one is analysis of a laminated annular plate consisting of one host layer of steel and two piezoelectric layers on the top and bottom surfaces of the host layer. Material properties for steel are $E = 200\,\mathrm{GPa}$, $v = 0.3$, and $\rho = 7800\,\mathrm{kg/m^3}$ and those for the piezoelectric material (PZT4) are also shown in Table 1. The host plates of steel with thicknesses 0.02 and 0.06 m are studied, which correspond to a thin and a thick plate when the inner and outer radii are of the same 0.1 and 0.6 m for both thicknesses. Piezoelectric layer has a thickness which is 1/20 of that of the host layer. These are example problems studied also by Duan et al. [9] with exact methods based on the classical plate theory and the Mindlin plate theory, and by ABAQUS 3-D finite element method. A convergence test with the present approach is first conducted and shown in Table 3. Convergence is considered reached when the discrepancy between two consecutive meshes is within 0.5%. From Table 3, a monotonic convergence is observed that the natural frequency becomes smaller when the mesh is finer. This is typical for all the boundary conditions and for both the thin and thick laminated plates. With these convergence trends in mind, those two laminated plates under four types of boundary conditions (c–c, c–s, s–c, s–s with c being clamped and s simply supported, the former one for inner edge and the latter outer edge) are analyzed and demonstrated in Table 4 (thick plate, mesh 20×10) and Table 5 (thin plate, mesh 50×6). Each piezoelectric layer is modeled as one layer of finite elements in both cases. Comparisons are being made with those in Ref. [9]. From Tables 4 and 5, we may find that the discrepancy of frequencies between the present results and those by the classical plate theory is greater for larger n (number of

Table 1
Properties of piezoelectric ceramic materials

	PIC-151 [16]	PZT4 [9]	PZT(NEPEC6) [20]
$\varepsilon^s_{11}/\varepsilon_0$	1111	804.6	730
$\varepsilon^s_{33}/\varepsilon_0$	925	659.7	635
$c^E_{11}(10^{10}\,\mathrm{N/m^2})$	10.76	13.2	13.9
c^E_{33}	10.04	11.5	11.5
c^E_{12}	6.313	7.1	7.78
c^E_{13}	6.386	7.3	7.43
c^E_{44}	1.962	2.6	2.56
c^E_{66}	2.224	3.05	3.06
e_{31} ($\mathrm{C/m^2}$)	−9.52	−4.1	−5.2
e_{33}	15.14	14.1	15.1
e_{15}	11.97	10.5	12.7
ρ ($10^3\,\mathrm{kg/m^3}$)	7.8	7.5	7.6

$\varepsilon_0 = 8.854 \times 10^{-12}\,\mathrm{F/m}$.

Table 2
Natural frequencies (Hz) for a piezoelectric circular plate under free boundary condition, n: number of nodal diameters, mesh 20×2, numbers in parentheses represent percentage difference compared to the present ones

n	Mode no.	Present	ABAQUS 3-D [16]	Experiment [16]
0	1	6985	6989(0.06%)	6050(−13.4%)
	2	27,844	27,924(0.29%)	25,550(−8.24%)
	3	64,368	64,368(0%)	70,500(9.52%)
	4	167,404	167,404(0%)	180,279(7.69%)
	5	265,152	265,147(0%)	288,900(8.96%)
	6	361,015	360,988(0%)	390,400(8.14%)
1	1	15,070	15,094(0.16%)	13,574(−9.93%)
2	1	3190	3192(0.06%)	3230(1.25%)
	2	25,087	25,157(0.28%)	23,060(−8.08%)
3	1	7481	7492(0.15%)	7568(1.16%)
4	1	13,174	13,204(0.23%)	13,310(1.03%)
5	1	20,177	20,243(0.33%)	20,257(0.39%)

Table 3
Convergence of natural frequencies (rad/s) for a laminated annular plate of steel (thickness 0.06 m) and piezoelectric ceramic layers under clamped–clamped boundary condition, n: number of nodal diameters, m: number of nodal circles

n	m	Mesh 20×3	20×6	20×10
0	0	7536	7439	7435
	1	18,865	18,527	18,515
	2	33,431	32,715	32,692
1	0	7848	7751	7746
	1	19,398	19,062	19,050
	2	33,799	33,314	33,291
2	0	9275	9176	9172
	1	21,264	20,922	20,912
	2	35,983	35,253	35,233

nodal diameters) and m (number of nodal circles), and for thicker plates under all the various boundary conditions. The classical plate theory overestimates vibration frequencies, as expected. However, when the Mindlin plate theory is applied to thin plates, frequencies derived are still higher than those of the present approach, and the difference is smaller for larger n and m. The Mindlin plate theory takes into account transverse shear deformation and rotary inertia which soften the plates and makes the vibration slower. These effects are more pronounced for higher modes (larger n and m) with all the four types of boundary conditions and that is justified from the relatively smaller differences compared with the present solutions. As the thick plates are concerned, remedies proposed by the Mindlin plate theory over the classical plate theory have even more effects of reducing vibration frequencies, and actually overshoot for higher modes under all the four boundary conditions except s–s. This can cause difficulties when judging if the Mindlin plate theory gives upper bound or lower bound solutions. However, the results of the Mindlin plate theory are still much better than those of the classical plate theory, based on comparisons with the present solutions, in all the cases studied. As to the ABAQUS 3-D solutions, which are supposed to be the lowest among the present method and the classical plate theory, are unanimously higher than the present ones with differences between 1% and 4%. From the convergence test in Table 3, it is clear that finer mesh leads to lower frequency. Therefore, a conjecture for the overestimations of ABAQUS results might be due to coarse finite element meshes used in Ref. [9] to derive ABAQUS 3-D solutions.

The third example is an analysis of the stator of a traveling wave ultrasonic motor which is designed to utilize the (0, 9) mode to produce the traveling wave. This is an example analyzed in Ref. [20] with the configuration of the stator and the arrangement of electrodes shown in Fig. 1, which is duplicated from

Table 4
Natural frequencies (rad/s) for a laminated annular plate of steel (thickness 0.06 m) and piezoelectric ceramic layers under different boundary conditions, n: number of nodal diameters, m: number of nodal circles, numbers in parentheses represent percentage difference compared to the present ones

B. C.	n	m	Present	ABAQUS 3-D [9]	Classical plate theory [9]	Mindlin plate theory [9]
c–c	0	0	7435	7608(2.3%)	8444(14%)	7416(−0.26%)
		1	18,515	18,828(1.7%)	23,358(26%)	18,235(−1.5%)
		2	32,692	33,096(1.2%)	45,917(40%)	31,869(−2.5%)
	1	0	7746	7918(2.2%)	8857(14%)	7728(−0.23%)
		1	19,050	19,358(1.6%)	24,089(26%)	18,774(−1.4%)
		2	33,291	33,685(1.2%)	46,824(41%)	32,468(−2.5%)
	2	0	9172	9336(1.8%)	10,571(15%)	9169(−0.033%)
		1	20,912	21,199(1.4%)	26,520(27%)	20,639(−1.3%)
		2	35,233	35,591(1.0%)	49,706(41%)	34,397(−2.4%)
c–s	0	0	5031	5171(2.8%)	5528(9.9%)	5064(0.66%)
		1	15,531	15,924(2.5%)	18,661(20%)	15,500(−0.20%)
		2	29,489	30,188(2.4%)	39,332(33%)	29,201(−0.98%)
	1	0	5369	5512(2.7%)	5950(11%)	5406(0.69%)
		1	16,070	16,464(2.4%)	19,376(20%)	16,048(−0.14%)
		2	30,104	30,803(2.3%)	40,232(34%)	29,827(−0.92%)
	2	0	6838	6990(2.2%)	7604(11%)	6907(1.0%)
		1	17,978	18,376(2.2%)	21,776(21%)	17,986(0.044%)
		2	32,110	32,806(2.2%)	43,101(34%)	31,854(−0.80%)
s–c	0	0	6045	6218(2.9%)	6647(10%)	6125(1.3%)
		1	16,469	16,939(2.8%)	19,845(20%)	16,536(0.41%)
		2	30,325	31,161(2.8%)	40,594(34%)	30,197(−0.42%)
	1	0	6479	6664(2.8%)	7337(13%)	6555(1.2%)
		1	17,126	17,593(2.7%)	20,949(22%)	17,172(0.27%)
		2	31,000	31,809(2.6%)	41,883(35%)	30,826(−0.56%)
	2	0	8470	8650(2.1%)	9707(15%)	8528(0.68%)
		1	19,496	19,909(2.1%)	24,357(25%)	19,453(−0.22%)
		2	33,291	33,990(2.1%)	45,821(38%)	32,959(−1.0%)
s–s	0	0	3912	4032(3.1%)	4187(7.0%)	3997(2.2%)
		1	13,547	14,030(3.6%)	15,593(15%)	13,775(1.7%)
		2	27,117	28,159(3.8%)	34,466(27%)	27,430(1.2%)
	1	0	4361	4498(3.1%)	4840(11%)	4450(2.0%)
		1	14,223	14,716(3.5%)	16,674(17%)	14,443(1.5%)
		2	27,822	28,852(3.7%)	35,753(28%)	28,102(1.0%)
	2	0	6332	6484(2.4%)	7064(12%)	6433(1.6%)
		1	16,688	17,162(2.8%)	20,008(20%)	16,859(1.0%)
		2	30,222	31,183(3.2%)	39,676(31%)	30,385(0.54%)

Ref. [20]. The stator is a laminated ring of brass and PZT with a poling pattern shown in Fig. 1. The brass has material properties $E = 100.6\,\text{GPa}$, $v = 0.35$, and $\rho = 8560\,\text{kg/m}^3$ and the material constants of PZT(NEPEC6) are shown in Table 1. The frequency of (0,9)-mode obtained by experiment and 3-D finite element steady-state response analysis in Ref. [20] are 45.672(kHz) and 45.682, respectively, compared with 45.898 of the present analysis. The discrepancy between the experiment and the present one is just a small 0.49%. The reason for the overestimation of the present solution might be due to the whole-ring-poling assumption of the piezoelectric layer in the present approach, while there are unpolarized regions in the real stator. Poling could lead to stiffening of a structure, the so-called 'piezoelectric stiffening' [14]. Another reason might be the existence of damping, however, it is generally of little effect on vibration frequency. It is also noteworthy that, by setting the number of nodal diameters $n = 9$, the frequency of (0,9)-mode is easily found in the present analysis, while in 3-D finite element analysis, it is hardwork to locate the frequency of a particular mode.

Table 5
Natural frequencies (rad/s) for a laminated annular plate of steel (thickness 0.02 m) and piezoelectric ceramic layers under different boundary condition on both inner and outer edges, n: number of nodal diameters, m: number of nodal circles, numbers in parentheses represent percentage difference compared to the present ones

B. C.	n	m	Present	ABAQUS 3-D [9]	Classical plate theory [9]	Mindlin plate theory [9]
c–c	0	0	2724	2812(3.2%)	2815(3.3%)	2769(1.6%)
		1	7418	7659(3.2%)	7786(5.0%)	7517(1.3%)
		2	14,289	14,753(3.2%)	15,306(7.1%)	14,428(0.97%)
	1	0	2853	2942(3.1%)	2952(3.5%)	2899(1.6%)
		1	7642	7882(3.1%)	8030(5.1%)	7743(1.3%)
		2	14,557	15,020(3.2%)	15,608(7.2%)	14,698(0.97%)
	2	0	3381	3471(2.7%)	3506(3.7%)	3438(1.7%)
		1	8394	8635(2.9%)	8840(5.3%)	8507(1.3%)
		2	15,416	15,877(3.0%)	16,569(7.5%)	15,566(0.97%)
c–s	0	0	1790	1848(3.2%)	1843(3.0%)	1823(1.8%)
		1	5967	6164(3.3%)	6220(4.2%)	6066(1.6%)
		2	12,357	12,770(3.3%)	13,111(6.1%)	12,523(1.3%)
	1	0	1922	1981(3.1%)	1983(3.2%)	1957(1.8%)
		1	6187	6384(3.2%)	6459(4.4%)	6289(1.6%)
		2	12,625	13,038(3.3%)	13,411(6.2%)	12,794(1.3%)
	2	0	2448	2511(2.6%)	2535(3.6%)	2495(1.9%)
		1	6934	7134(2.9%)	7259(4.7%)	7050(1.7%)
		2	13,490	13,903(3.1%)	14,367(6.5%)	13,672(1.3%)
s–c	0	0	2152	2213(2.8%)	2216(3.0%)	2194(2.0%)
		1	6345	6544(3.1%)	6615(4.2%)	6455(1.7%)
		2	12,755	13,169(3.2%)	13,531(6.1%)	12,934(1.4%)
	1	0	2352	2418(2.8%)	2446(4.0%)	2397(1.9%)
		1	6663	6865(3.0%)	6983(4.8%)	6774(1.7%)
		2	13,112	13,528(3.2%)	13,961(6.5%)	13,293(1.4%)
	2	0	3102	3178(2.4%)	3236(4.3%)	3159(1.8%)
		1	7692	7902(2.7%)	8119(5.6%)	7815(1.6%)
		2	14,243	14,663(2.9%)	15,274(7.2%)	14,428(1.3%)
s–s	0	0	1358	1395(2.7%)	1396(2.8%)	1388(2.2%)
		1	5014	5173(3.2%)	5198(3.7%)	5115(2.0%)
		2	10,921	11,283(3.3%)	11489(5.2%)	11,114(1.8%)
	1	0	1551	1593(2.7%)	1613(4.0%)	1583(2.1%)
		1	5328	5490(3.0%)	5558(4.3%)	5433(2.0%)
		2	11,283	11,647(3.2%)	11,918(5.6%)	11,478(1.7%)
	2	0	2260	2312(2.3%)	2355(4.2%)	2306(2.0%)
		1	6348	6521(2.7%)	6669(5.0%)	6468(1.9%)
		2	12,428	12,798(3.0%)	13,225(6.4%)	12,632(1.6%)

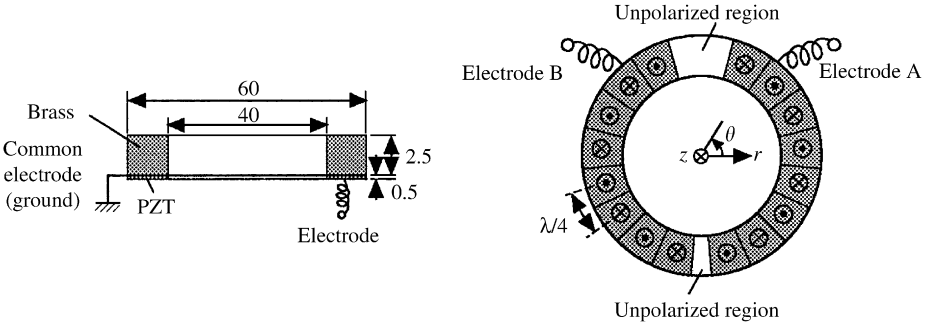

Fig. 1. Stator configuration and electrode arrangement for ninth flexural mode excitation. Units in mm. Polarization direction: ⊕, z-axis positive; ⊙, z-axis negative (same as Fig. 2 in Ref. [20]).

Considering the accurate results of the present approach shown in the above three analyses, the accuracy of the present approach can thus be validated. Besides, vibration of piezoelectric circular or annular plates is analyzed with the number of nodal diameters preselected in the present formulation. This is a feature especially suitable for the design work of traveling wave ultrasonic motors where only a few of frequencies and modes with particular circumferential wave numbers are of interest, and it also offers the advantage to perform 3-D analyses with a 2-D finite element.

4. Conclusions

In the present research, a modified axisymmetric finite element is proposed. The finite element takes into account the electromechanical effects and has the capability to conduct 3-D axisymmetric and nonaxisymmetric vibration analysis of piezoelectric laminated circular and annular plates. The present approach is totally based on the 3-D electroelasticity with the only assumption that the motion of the plates is temporally and circumferentially harmonic. A special feature of the present formulation is that 3-D vibration behaviors of piezoelectric circular plates can be analyzed with a 2-D finite element when the circumferential wave number is chosen. This is especially useful for the analysis of stator of traveling wave ultrasonic motor where only vibration frequencies and modes with some particular circumferential wave numbers are of interest.

Validity and accuracy of the present approach are confirmed by comparing the present results of three example problems to those in literature—one being a piezoelectric circular plate, another dealing with a thin and a thick laminated annular plates of piezoelectric ceramics and steel, and the third one is the analysis of the stator of a traveling wave ultrasonic motor. For the entirely piezoelectric circular plate case, solutions of vibration frequencies by the present method are in excellent agreement with 3-D results by ABAQUS, so is the case of the stator analysis with experiment result. While in the laminated plate cases, the present solutions are compared with those by the classical plate theory, the Mindlin plate theory, and ABAQUS 3-D finite element. Although discrepancies exist among these methods, they can be explained properly and satisfactorily.

Owing to the numerous possibilities of combinations of materials and geometric aspect ratios, the conclusions drawn from the example problems should not be over-stretched. Analysis might be needed for each particular problem, and in that case, the present method can be considered a convenient and practical alternative when vibration of circular and annular laminated piezoelectric plates is concerned.

Appendix

$$[k_{uu}] = \begin{bmatrix} k^{11} & k^{12} & k^{13} \\ k^{21} & k^{22} & k^{23} \\ k^{31} & k^{32} & k^{33} \end{bmatrix}, \quad [m_{uu}] = \begin{bmatrix} m^{11} & 0 & 0 \\ 0 & m^{22} & 0 \\ 0 & 0 & m^{33} \end{bmatrix}, \quad [k_{u\varphi}] = \begin{bmatrix} k^{14} \\ k^{24} \\ k^{34} \end{bmatrix},$$

$$(k^{11})_{ij} = \int (c_{11}N_{i,r}N_{j,r} + c_{12}N_{i,r}N_j/r + c_{12}N_iN_{j,r}/r + c_{11}N_iN_j/r^2 + c_{44}N_{i,z}N_{j,z} + c_{66}n^2N_{i,z}N_{j,z}/r^2)\pi r\,\mathrm{d}r\,\mathrm{d}z,$$

$$(k^{12})_{ij} = \int (c_{12}nN_{i,r}N_j/r - c_{66}nN_iN_{j,r}/r + c_{11}nN_iN_j/r^2 + c_{66}nN_iN_j/r^2)\pi r\,\mathrm{d}r\,\mathrm{d}z,$$

$$(k^{13})_{ij} = \int (c_{13}N_{i,r}N_{j,z} + c_{13}N_iN_{j,z}/r + c_{44}N_{i,z}N_{j,r})\pi r\,\mathrm{d}r\,\mathrm{d}z,$$

$$(k^{22})_{ij} = \int (c_{11}n^2N_iN_j/r^2 + c_{44}N_{i,z}N_{j,z} + c_{66}N_{i,r}N_{j,r} - c_{66}N_{i,r}N_j/r - c_{66}N_iN_{j,r}/r + c_{66}N_iN_j/r^2)\pi r\,\mathrm{d}r\,\mathrm{d}z,$$

$$(k^{23})_{ij} = \int (c_{13} n N_i N_{j,z}/r - c_{44} n N_{i,z} N_j/r)\pi r \,\mathrm{d}r \,\mathrm{d}z,$$

$$(k^{33})_{ij} = \int (c_{33} N_{i,z} N_{j,z} + c_{44} N_{i,r} N_{j,r} + c_{44} n^2 N_i N_j/r^2)\pi r \,\mathrm{d}r \,\mathrm{d}z,$$

$$(k^{21})_{ji} = (k^{12})_{ij}, \quad (k^{31})_{ji} = (k^{13})_{ij}, \quad (k^{32})_{ji} = (k^{23})_{ij},$$

$$(m^{pp})_{ij} = \rho \int (N_i N_j)\pi r \,\mathrm{d}r \,\mathrm{d}z, \quad p = 1-3,$$

$$(k^{14})_{ij} = \int (e_{15} N_{i,z} N_{j,r} + e_{31} N_{i,r} N_{j,z} + e_{31} N_i N_{j,z}/r)\pi r \,\mathrm{d}r \,\mathrm{d}z,$$

$$(k^{24})_{ij} = \int (-e_{15} n N_{i,z} N_j/r + e_{31} n N_i N_{j,z}/r)\pi r \,\mathrm{d}r \,\mathrm{d}z,$$

$$(k^{34})_{ij} = \int (e_{15} N_{i,r} N_{j,r} + e_{15} n^2 N_i N_j/r^2 + e_{33} N_{i,z} N_{j,z})\pi r \,\mathrm{d}r \,\mathrm{d}z,$$

$$[k_{\phi\phi}] = (k_{\phi\phi})_{ij} = -\int (\varepsilon_{11} N_{i,r} N_{j,r} + \varepsilon_{11} n^2 N_i N_j/r^2 + \varepsilon_{33} N_{i,z} N_{j,z})\pi r \,\mathrm{d}r \,\mathrm{d}z,$$

where $i, j = 1$–nd.

References

[1] Q. Wang, S.T. Quek, C.T. Sun, X. Liu, Analysis of piezoelectric coupled circular plate, *Smart Materials and Structures* 10 (2001) 229–239.

[2] C.H. Huang, Transverse vibration analysis and measurement for the piezoelectric annular plate with different boundary conditions, *Journal of Sound and Vibration* 283 (2005) 665–683.

[3] P. Hagedorn, J. Wallaschek, Travelling wave ultrasonic motors, part 1: working principle and mathematical modeling of the stator, *Journal of Sound and Vibration* 155 (1) (1992) 31–46.

[4] N. Hagood, A. McFarland, Modeling of a piezoelectric rotary ultrasonic motor, *IEEE Transactions on Ultrasonics, Ferroelectrics, and Frequency Control* 42 (2) (1995) 210–224.

[5] P. Hagedorn, T. Sattel, D. Speziari, J. Schmidt, G. Diana, The importance of rotor flexibility in ultrasonic traveling wave motors, *Smart Materials and Structures* 7 (1998) 352–368.

[6] J. Friend, D. Stutts, The dynamics of an annular piezoelectric motor stator, *Journal of Sound and Vibration* 204 (3) (1997) 421–437.

[7] Y. Ming, Q. Peiwen, Performance estimation of a rotary traveling wave ultrasonic motor based on two-dimension analytic model, *Ultrasonics* 39 (2001) 115–120.

[8] X. Liu, Q. Wang, S.T. Quek, Analytical solution for free vibration of piezoelectric coupled moderately thickness circular plates, *International Journal of Solids and Structures* 39 (2002) 2129–2151.

[9] W.H. Duan, S.T. Quek, Q. Wang, Free vibration analysis of piezoelectric coupled thin and thick annular plate, *Journal of Sound and Vibration* 281 (2005) 119–139.

[10] Y. Kagawa, T. Yamabuchi, Finite element approach for a piezoelectric circular rod, *IEEE Transactions on Sonics and Ultrasonics* SU-23 (6) (1976) 379–385.

[11] N.T. Adelman, Y. Stavsky, E. Segal, Axisymmetric vibrations of radially polarized piezoelectric ceramic cylinders, *Journal of Sound and Vibration* 38 (1975) 245–254.

[12] N. Guo, P. Cawley, D. Hitchings, The finite element analysis of the vibration characteristics of piezoelectric discs, *Journal of Sound and Vibration* 159 (1) (1992) 115–138.

[13] H.A. Kunkel, S. Locke, B. Pikeroen, Finite-element analysis of vibrational modes in piezoelectric ceramic disks, *IEEE Transactions on Ultrasonics, Ferroelectrics, and Frequency Control* 37 (4) (1990) 316–328.

[14] P.R. Heyliger, G. Ramirez, Free vibration of laminated circular piezoelectric plates and discs, *Journal of Sound and Vibration* 229 (4) (2000) 935–956.

[15] H. Ding, R. Xu, Y. Chi, W. Chen, Free axisymmetric vibration of transversely isotropic piezoelectric circular plates, *International Journals of Solids and Structures* 36 (1999) 4629–4652.

[16] Y.C. Lin, C.C. Ma, Experimental measurement and numerical analysis on resonant characteristics of piezoelectric disks with partial electrode designs, *IEEE Transactions on Ultrasonics, Ferroelectrics, and Frequency Control* 54 (8) (2004) 937–947.
[17] C.F. Liu, Y.T. Lee, Finite element analysis of three-dimensional vibrations of thick circular and annular plates, *Journal of Sound and Vibration* 233 (1) (2000) 63–80.
[18] K. Uchino, Piezoelectric ultrasonic motors: overview, *Smart Materials and Structures* 7 (1998) 273–285.
[19] H. Allik, T.J.R. Hughes, Finite element method for piezoelectric vibration, *International Journal for Numerical Methods in Engineering* 2 (1970) 151–157.
[20] Y. Kagawa, T. Tsuchiya, T. Kataoka, T. Yamabuchi, T. Furukawa, Finite element simulation of dynamic responses of piezoelectric actuators, *Journal of Sound and Vibration* 191 (4) (1996) 519–538.